



# Numerical Investigation in the Vaned Distributor under Different Guide Vanes Openings of a Pump Turbine in Pump Mode

D. Y. Li<sup>1</sup>, R. Z. Gong<sup>1</sup>, H. J. Wang<sup>1†</sup>, J. Zhang<sup>1</sup>, X. Z. Wei<sup>1,2</sup> and L. F. Shu<sup>3</sup>

<sup>1</sup> School of Energy Science and Engineering, Harbin Institute of Technology, Harbin, Heilongjiang, 150001, China

<sup>2</sup> State Key Laboratory of Hydro-Power Equipment, Harbin Institute of Large Electrical Machinery, Harbin, Heilongjiang, 150040, China

<sup>3</sup> Huadong Engineering Corporation Limited, Zhejiang, Hangzhou, 310014, China

†Corresponding Author Email: [wanghongjie@hit.edu.cn](mailto:wanghongjie@hit.edu.cn)

(Received November 8, 2014; accepted January 12, 2015)

## ABSTRACT

The performance of a pump turbine in pump mode is of great importance to a pumped storage power plant. In order to obtain pump characteristics of a pump turbine, 3D steady simulations were carried out by solving Reynolds-averaged Navier-Stokes (RANS) equations using different two-equation turbulence models. Compared with the experimental data, SST  $k-\omega$  turbulence model was chosen to simulate external characteristic curves under 32mm, 22mm and 18mm guide vanes openings. The results show a good agreement with the experimental data, especially near the best efficiency point. Finally, the detailed analysis was conducted within vaned distributor for these three guide vanes openings. The variation of flow field, pressure field, energy characteristic and loss with the discharge and guide vanes opening were obtained through the analysis. This research could provide a basic understanding on pump characteristics of a pump turbine for designer.

**Keywords:** Hydraulic machinery; Pump turbine; Numerical investigation; Vaned distributor; Pump mode.

## NOMENCLATURE

BEP	best efficiency point under one guide vanes opening	$y^+$	dimensional wall distance
H	head of the pump turbine in pump mode (m)	$\eta$	efficiency of the pump turbine
Q	mass flow rate (kg/s)	$u_i$	average velocity component
QBEP1	mass flow rate of best efficiency point under 32mm guide vanes opening (kg/s)	$\overline{u_i u_j}$	the turbulent stress
QBEP2	mass flow rate of best efficiency point under 22mm guide vanes opening (kg/s)	$k$	turbulent kinetic energy
QBEP3	mass flow rate of best efficiency point under 18mm guide vanes opening (kg/s)	$\omega$	turbulent dissipation rate

## 1. INTRODUCTION

Hydropower is the major renewable energy according to IEA (International Energy Agency 2012) worldwide. Among the hydropower, pumped storage power plant develops rapidly due to its effective electric storage and generation. As for a pumped storage power plant, a pump turbine is the most important part, whose safe and stable operation is the key for the whole plant. However, the existence of a positive slope in the external

characteristic curve (head-discharge) would lead to operation instability and limit operating range. This characteristic is well known as the hump characteristic. In order to ensure safe and effective operation, it is significantly important to analyze the energy characteristic of a pump turbine in pump mode, especially for different guide vanes openings.

Presently, lots of studies have been carried out to investigate hydraulic performance of pump turbines. Liu *et al.* (2012) predicted hump characteristic curves using an improved cavitation

model, and concluded that the hump characteristic has a certain relation with cavitation. They (2013) also studied unsteady cavitation flow and pressure fluctuation of the pump turbine in pump mode based on above model. Similar work was also carried out by Anciger (2010), He demonstrated rotating stall phenomenon and cavitation region in pump turbines. Moreover, Li *et al.* (2015) conducted unsteady simulation using SST  $k-\omega$  turbulence model to investigate hump characteristics and concluded that the cause of hump is related to vortex in the tandem cascade. Other three dimensional unsteady simulations were also undertaken. Hasmatuchi (2010) and Yan (2012) proposed that one stall cell rotating with the runner in a subsynchronous rotating velocity is main cause for flow separation and flow passages blockage of a pump turbine in turbine mode. There are some other investigations in pump turbines. Yan (2010) mentioned that numerical results using compressible turbulence model are closer to the experimental data. Premkumar (2014) carried out some studies for S shaped blade in pump turbine. Zuo (2015) reviewed pressure fluctuations in the vaneless space of high-head pump-turbines.

Based on the review from above literatures, little research for energy-discharge characteristic has been carried out. Flow mechanism of a pump turbine in pump mode is still not clear. Braun *et al.* (2005) studied unstable energy-discharge characteristics of an industrial pump turbine in pump mode and concluded that flow patterns, energy and velocity distribution at the rotor-stator interface are related to the onset of recirculation, However, they only analyzed one guide vanes opening just using one channel per component. Yin *et al.* (2010) also carried out some similar work to predict the performance and flow pattern of a pump turbine in pump mode, but this analysis was undertaken just in the vaned distributor at low flow rate at one guide vanes opening.

Detailed analysis for different discharge under different guide vanes openings of a pump turbine in pump mode has been not proposed. As for a pump turbine, vaned distributor is the vital component. Hence, in this research, numerical simulations were conducted under three guide vanes openings of 18mm, 20mm and 32mm using SST  $k-\omega$  turbulence model to investigate performance for different discharge including flow field, pressure field, energy characteristic as well as loss distribution. Compared with available experimental data, there shows a good agreement for external characteristic curves.

## 2. PUMP TURBINE SPECIFICATION AND EXPERIMENTAL SETUP

The investigated pump turbine model in the present work was installed in HEC (Harbin Institute of Electrical Machinery), Harbin, China. The test rig and scaled down (1:5) model is shown in Fig. 1.

Experimental measurements were carried out using closed loop water circuit. The closed loop test rig

design allows for both turbine and pump performance assessment within accuracy of 0.2%. Its main characteristics are summarized in Table 1. The measurement system was programmed by LabVIEW software.



Fig. 1. Pump turbine model test rig installed at HEC, China.

Table 1 Test rig parameters

Characteristics	Value
Maximum head (m)	80
Maximum discharge (m <sup>3</sup> /s)	0.8
Runner diameter range (mm)	300~500
Generating power (kW)	750
The test rig accuracy	0.20%

## 3. NUMERICAL MODEL

### 3.1 Computational Domain

The computational domain presents the pump turbine model, from the draft tube to the spiral casing as shown in Fig. 2. Four main parts are as follows: spiral casing, vaned distributor (stay-guide vanes), runner as well as draft tube. Table 2 gives the basic parameters of the pump turbine.



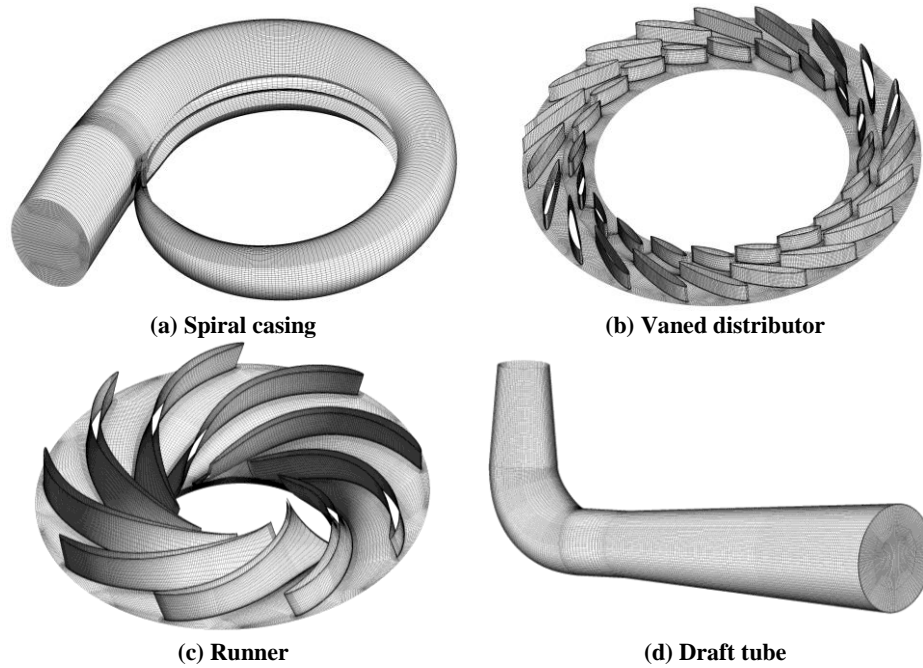
Fig. 2. Computational domain.

Table 2 Parameters of the pump turbine

Parameters	Value
Diameter of runner outlet (mm)	524
Diameter of runner inlet (mm)	274
Number of runner blades	9
Number of stay vanes	20
The height of guide vane (mm)	45.77
Number of guide vanes	20

### 3.2 Grid Generation

Structured hexahedral grids were generated for each



**Fig. 4. The grids of different parts.**

part employed ANSYS ICEM. In order to capture the flow separation of guide vanes, stay vanes as well as runner, the first node was placed at 0.003mm away from the wall of vanes and runner blades. Moreover,  $y^+$  at the wall layer is less than 2. The detail information of grid quality is given in Table 3. The quality of the structure grid is an aggregative indicator of the mesh orthogonal angle, expansion factor, aspect ratio and so on. The value of the grid quality ranges from 0 to 1. The higher value means higher grid quality. The grids for different parts are shown in Fig. 4.

**Table 3 The quality of grid**

Component	Quality
Spiral casing	0.37
Vaned distributor	0.49
Runner	0.56
Draft tube	0.61

### 3.3 Numerical Scheme

3D steady incompressible numerical simulations were performed using ANSYS CFX 14.0. Two-equation viscosity turbulence models were chosen for closure of the Navier-Stokes equations. High resolution scheme was used for advection term and 1<sup>st</sup> order upwind scheme for the other terms. The static pressure inlet for draft tube was used in pump mode, and the discharge outlet was specified for spiral casing according to experimental data. No slip wall conditions were used for solid walls. General Grid Interface (GGI) was used on the interfaces that separate the rotating and stationary domains, as well as any adjacent domain components. Besides, the frame change was set as stage for the rotating and stationary domains, which is most appropriate when the circumferential variation of the flow is of the order of the component pitch.

### 3.4 Grid Sensitivity

As for the pump turbine in pump mode, the most concerned parameters are head and efficiency. Hence, head and efficiency were chosen for grid sensitivity validation. Best efficiency point (QBEP2) under 22mm guide vanes opening was chosen for validation due to its operation condition is stable and simulation accuracy is high. Fig. 5 shows the head and efficiency of the pump turbine from simulations and experiments for five sets of grids with different mesh nodes. It is noted that the relative difference for all five sets is less than 3% and decreases with the mesh nodes increasing. When the mesh is increased above 5 million, the relative difference changes little. The deviation of calculated head and efficiency with 9.12 million nodes is less than 0.12% and 0.22% respectively compared with 5.45 million nodes. Finally, 5.46 million nodes were chosen to perform the simulations with considering simulation accuracy and time consuming.

### 3.5 Selection of Turbulence Model Validation

In order to choose the most suitable two-equation turbulence model, three dimensional steady simulations for different turbulence models including SST  $k-\omega$ , RNG  $k-\epsilon$ , Standard  $k-\epsilon$ , and Standard  $k-\omega$  were carried out at different mass flow rate operation conditions under 18 guide vanes opening. The results compared with experimental data were shown in Fig. 6. It can be seen from the figures that, the simulation accuracy is nearly the same for these four turbulence models around high efficiency operation conditions. However, the results of SST  $k-\omega$  turbulence are closer to the experiments at off-design conditions. Hence, in this research, SST  $k-\omega$  turbulence was chosen to

perform the simulations.

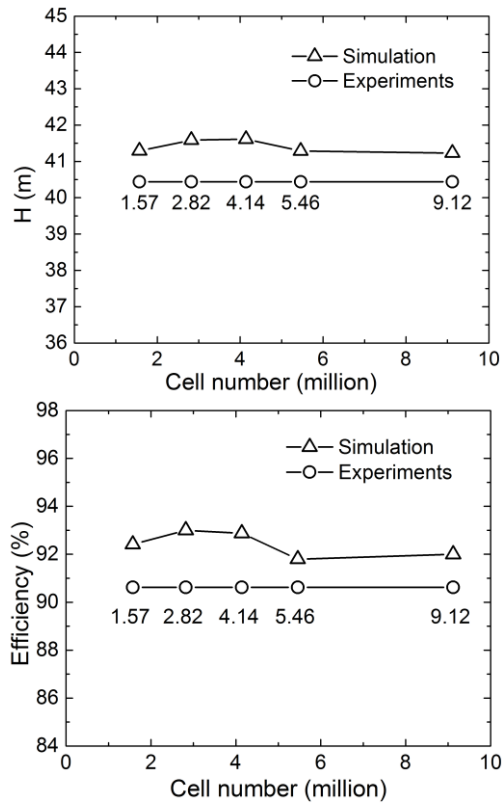


Fig. 5. Grid sensitivity validation (Head, Efficiency).

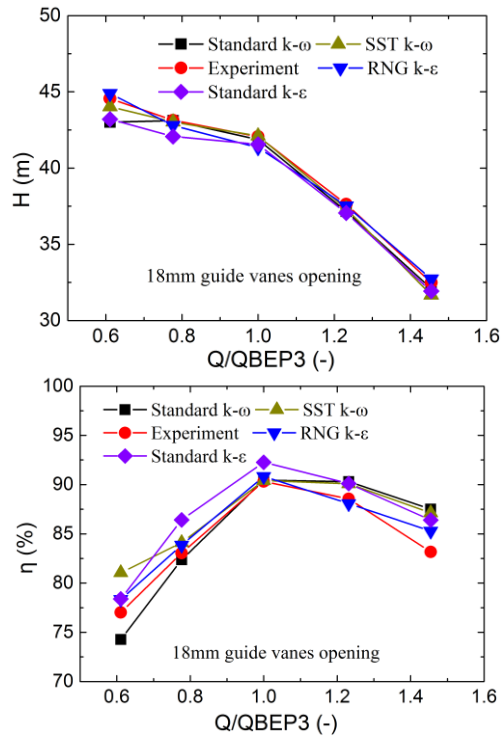


Fig. 6. The comparison of different turbulence models.

For steady incompressible turbulence flow the continuity equation and momentum equation can be

written as

$$\frac{\partial u_i}{\partial x_i} = 0 \quad (1)$$

$$\frac{1}{\rho} \frac{\partial p}{\partial x_i} + u_i \frac{\partial u_i}{\partial x_j} = \nu \frac{\partial^2 u_i}{\partial x_j \partial x_i} - \frac{\partial}{\partial x_j} (\overline{u_i u_j}) + F_i \quad (2)$$

The closure mode of SST  $k-\omega$  is listed as follows (Choi 2013):

$$\frac{\partial}{\partial x_i} (\rho \omega u_i) = \frac{\partial}{\partial x_i} \left( \Gamma_\omega \frac{\partial \omega}{\partial x_j} \right) + G_\omega - Y_\omega + D_\omega + S_\omega \quad (3)$$

$$\frac{\partial}{\partial x_i} (\rho k u_i) = \frac{\partial}{\partial x_i} \left( \Gamma_k \frac{\partial k}{\partial x_j} \right) + \overline{G_k} - Y_k + S_k \quad (4)$$

where  $k$  and  $\omega$  are turbulent kinetic energy and turbulence dissipation rate, respectively.  $G_\omega$  and  $\overline{G_k}$  are production term of the turbulence dissipation rate and turbulence kinetic energy.  $\Gamma_\omega$  and  $\Gamma_k$  are the effective diffusion coefficients of  $k$  and  $\omega$ , respectively.  $Y_\omega$  and  $Y_k$  are the dissipation terms.

$D_\omega$  is the cross diffusion tem, and  $S_\omega$  as well as  $S_k$  are source terms. The SST  $k-\omega$  turbulence model shows good behavior in adverse pressure gradients and separating flow. Moreover, SST  $k-\omega$  turbulence model does not produce too large turbulence levels in regions with large normal strain, such as stagnation regions and regions with strong acceleration. So, in this research, it shows better results at off-design conditions than other turbulence models.

## 4. RESULTS ANALYSIS

### 4.1 External characteristic validation

According to experimental data, several points at 18mm, 22mm and 32mm guide vanes opening were simulated. The results are shown in Fig. 7. BEP1, BEP2 and BEP3 stand best efficiency points for 32mm, 22mm and 18mm guide vanes openings, respectively. QBEP1, QBEP2 and QBEP3 denote the discharge corresponding to best efficiency points.

Fig. 7 shows the external characteristic curves of numerical results compared with the experimental data. From external characteristic curves under different guide vanes openings, they show a good agreement with the experimental data. The relative difference between the simulations and experiments is less than 1.5% during the high efficiency region. The highest relative difference is less than 5%, which usually occurs in the large discharge region, small discharge region or hump region. It can be seen from Fig. 7 that the highest efficiency value decreases and the high efficiency region becomes

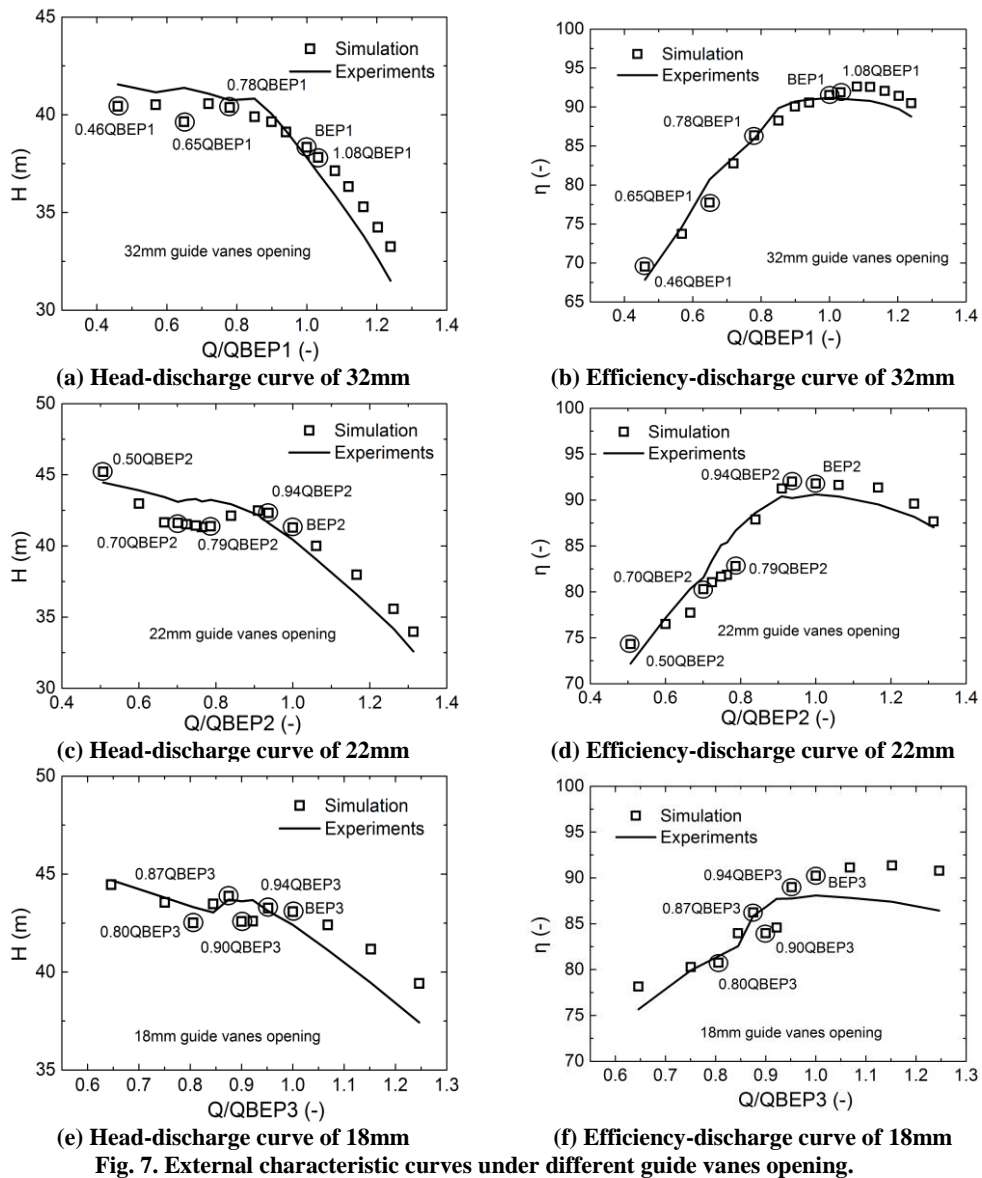


Fig. 7. External characteristic curves under different guide vanes opening.

narrow with the guide vanes opening reducing. In addition, the hump characteristic is more obvious under small guide vanes opening, but the hump region turns small. For each guide vanes opening, five operating condition points are chosen to analyze in the following (see Fig. 7-a, c and e).

#### 4.2 Detailed Analysis

The specific notations used in flow field analysis were depicted in Fig. 8. Blade-to-blade locations from crown to band were defined from 0 to 1 in the spanwise direction. Four cross-sections were defined on the runner inlet, runner outlet, guide vanes outlet and stay vanes outlet (pump mode) in the streamwise direction, respectively, as shown in Fig. 8.

As for a pump turbine, vaned distributor (stay-guide vanes) is one of the most important parts. In this region, the kinetic energy of flow is converted to pressure energy. The pressure at the stay vanes outlet increases, and the loss increases.

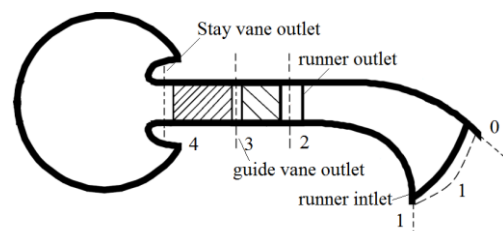


Fig. 8. Schematic of cross-sections studied in flow analysis.

In order to obtain the performance under different guide vanes openings, the investigation for vaned distributor was carried out in this research. Fig. 9 presents the velocity vectors of different flow surfaces near the best efficiency point (1.08 QBEP1) at 32mm guide vanes opening. Streamlines are all agreeable with the profile of stay-guide vanes, and no flow separation could be observed near the solid surfaces. At this operating condition, velocity is relative low and pressure shows high on

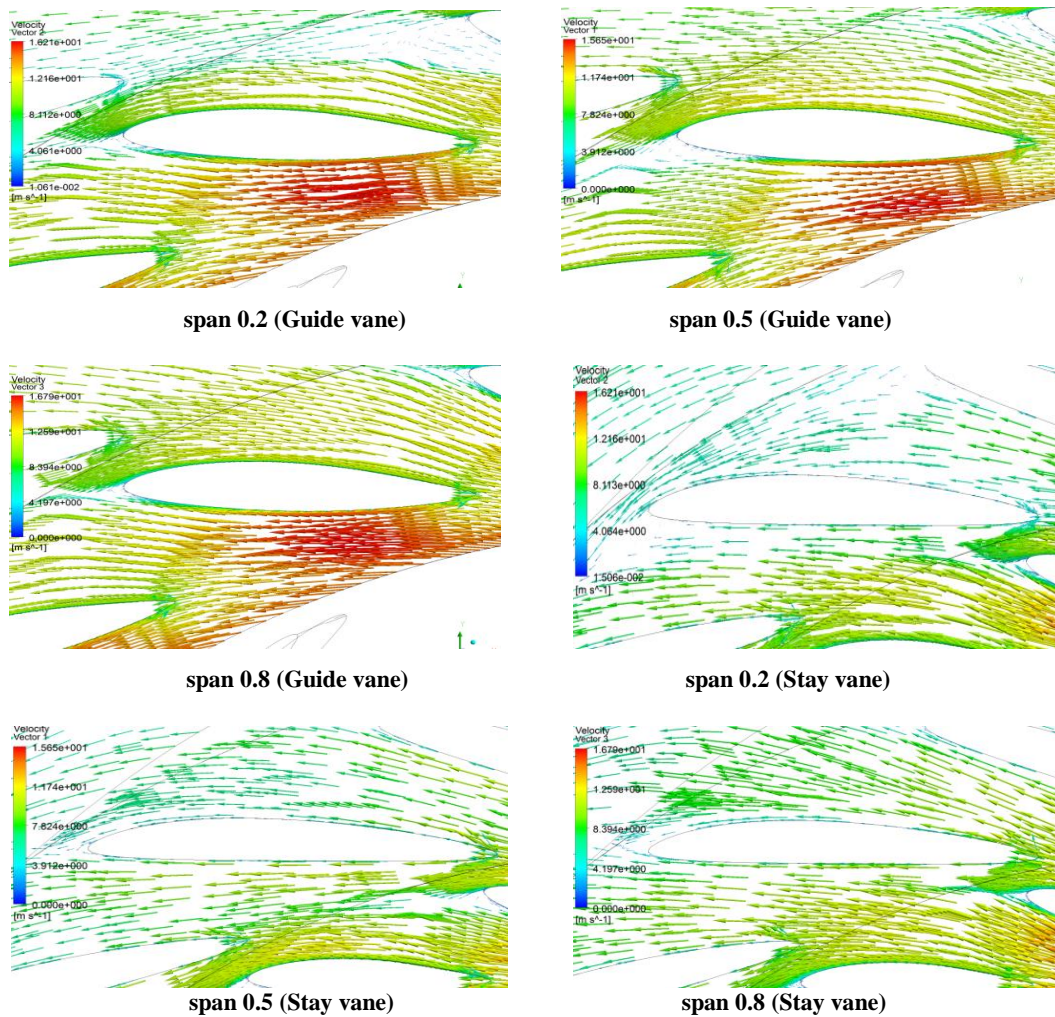


Fig. 9. Velocity vectors of different flow surfaces at 1.08 QBEP1 operating condition (32mm)

the suction surfaces of stay-guide vanes, vice versa on the pressure surfaces. This phenomenon could be explained that a small gap formed between guide vanes trails and stay vanes heads leads to acceleration of fluid, then vortex could be observed near the trailing points of guide vanes. The range of this vortex is so small that there is no large influence on flow field. As for stay vanes, only a small wake region can be found on the trail region from Fig. 9.

When the discharge is reduced to 0.78QBEP1, flow field of special stay vane and other parts of vane distributor is shown in Fig. 10. Numerical simulations show that flow field of special stay vane becomes badly first and turns worse from the band to the crown. This is because two sides of special stay vane are spiral casing inlet and trail. At the spiral casing outlet, pressure shows high and the total pressure of main flow is relative high. Furthermore, the space of spiral casing trail is small, which blocks the fluid. Hence, the resistance of fluid near the special stay vane is relative large, finally which leads to disorder flow.

With respect to other positions of vane distributor, near the crown, the vortex on the trails of guide

vanes turns out much bigger and two vortexes with different rotating direction can be found near the suction surfaces of stay vanes. The vortex blocks flow and leads to the fluid flow from gap passages, so the inlet attack angle on the gap passages of stay vanes increases, then flow separation and backflow occur on the heads of pressure surfaces of stay vanes.

When the discharge continues to decrease, the bad flow pattern spreads to other positions from special stay vane shown in Figs. 11 and 12. The position of bad flow pattern varies with discharge of runner outlet and the range becomes larger as discharge decreasing. Moreover, a large area of backflow can be founded in the vane distributor. In addition, the discharge distribution shows nonuniform on the different flow surfaces, so the fluid will flow from the high discharge surface to low discharge surface. This will generate secondary flow on the outlet of vane distributor and cause nonuniform pressure distribution (the lowest in the middle section) on the circumferential section (see Fig. 13). Hence, as shown in Fig. 14, secondary flow and main flow form helical flow pattern in stay vanes.

The mass average total pressure energy of runner

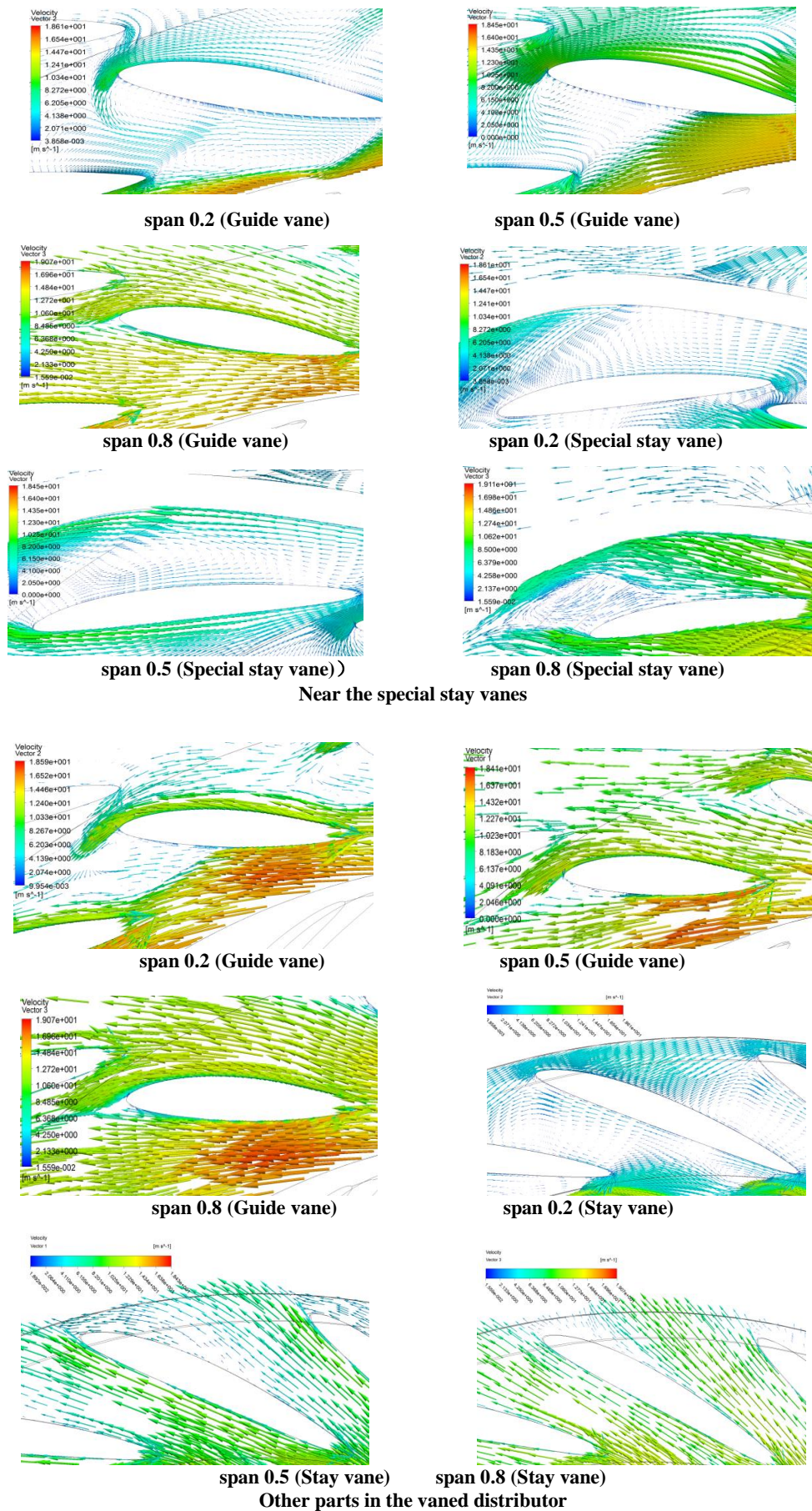


Fig. 10. Velocity vectors of different flow surfaces at 0.78QBEP1 operating condition (32mm).

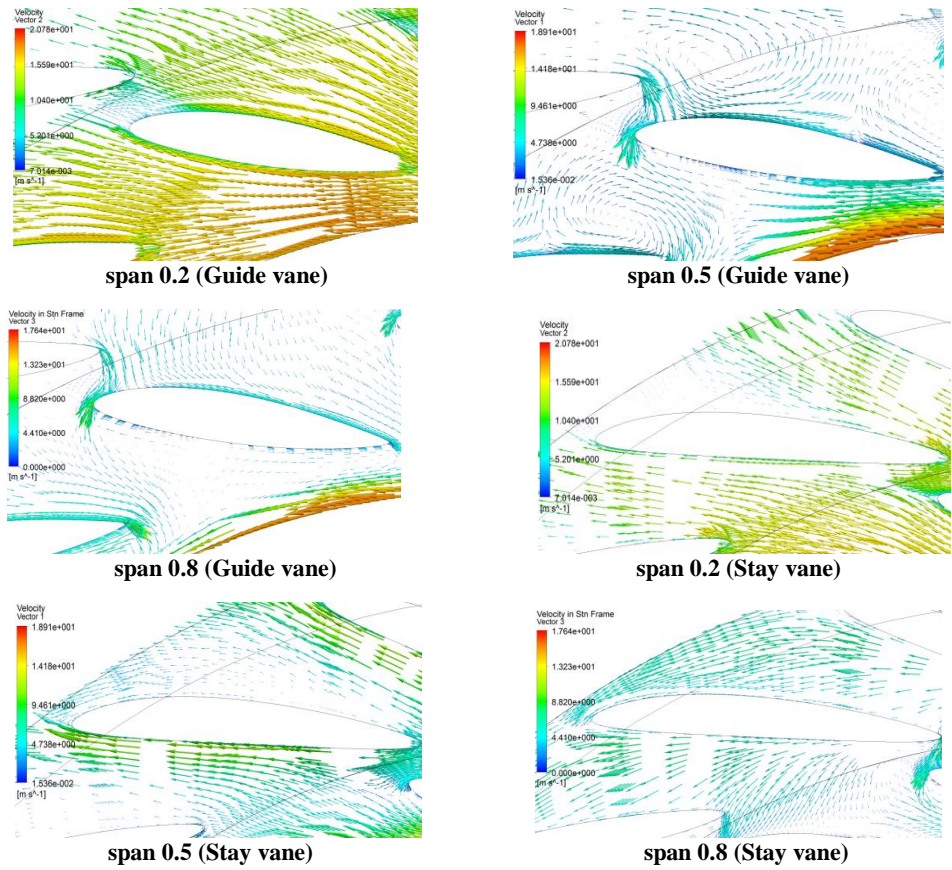


Fig. 11. Velocity vectors of different flow surfaces at 0.65QBEP1 operating condition (32mm).

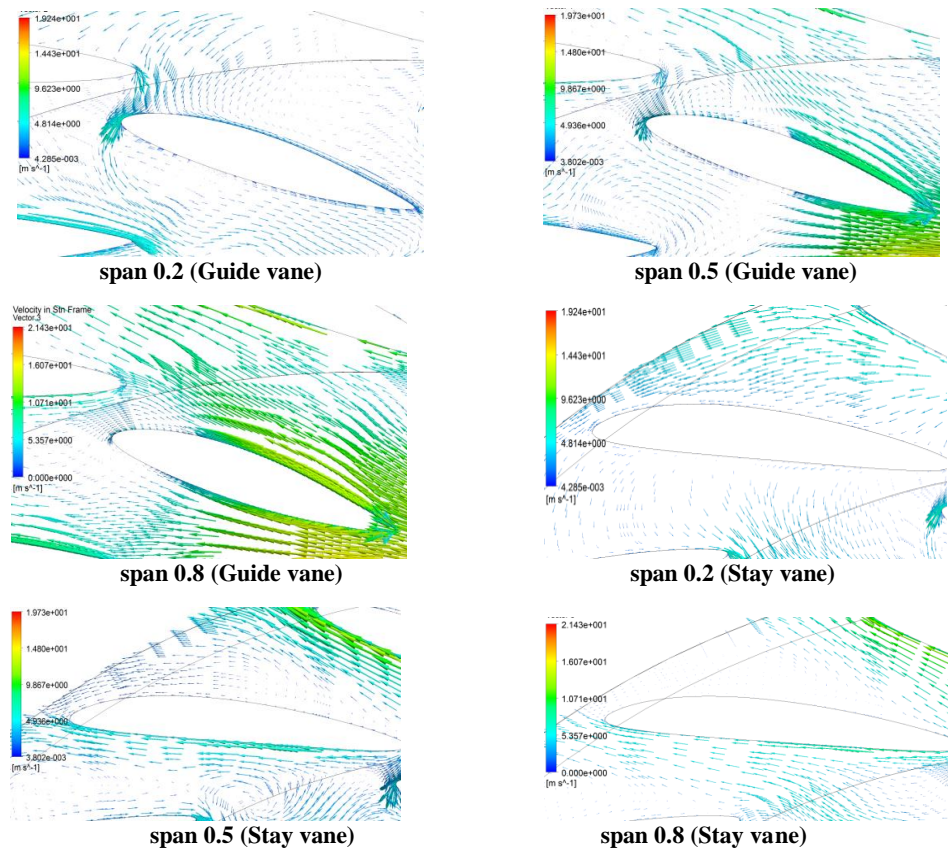
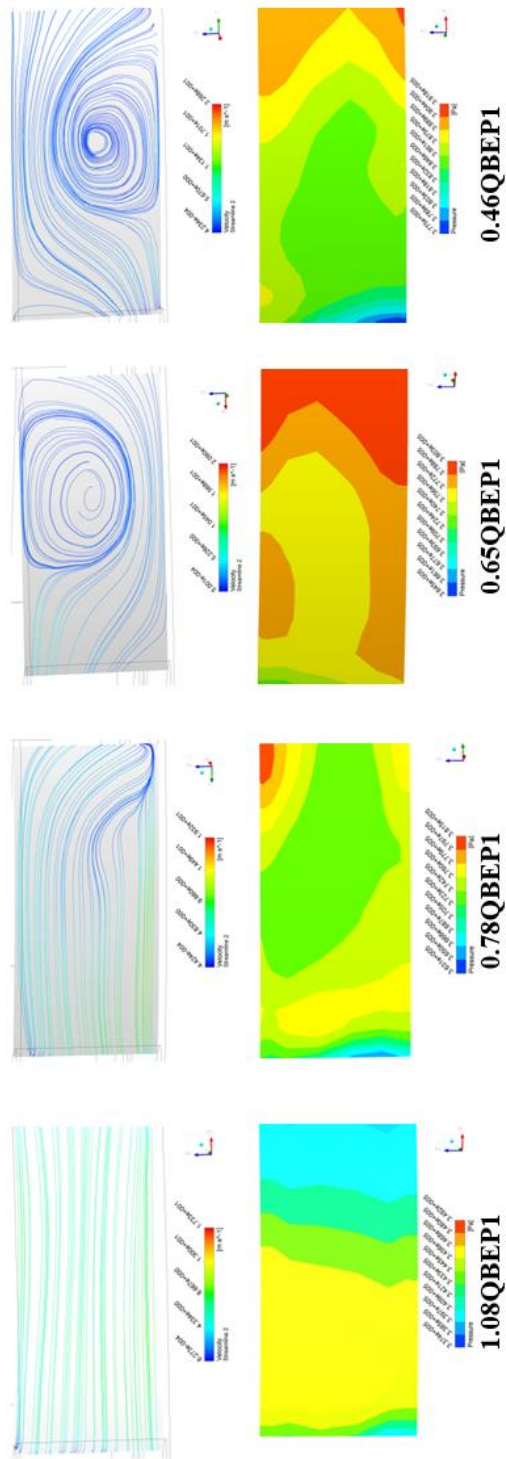
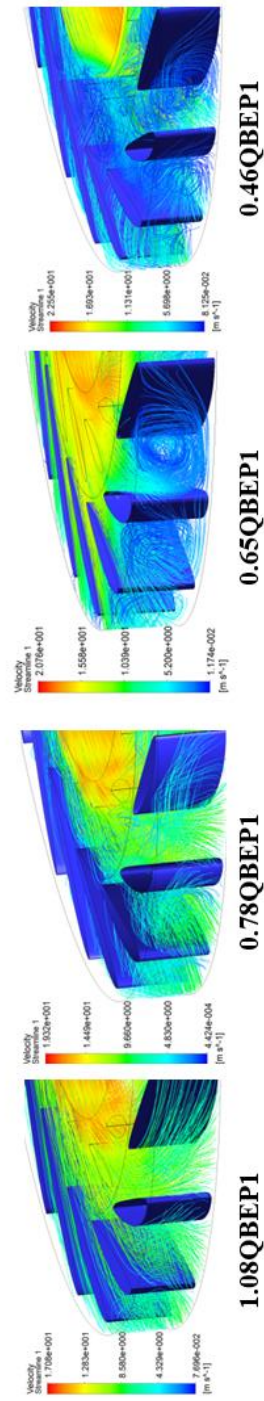


Fig. 12. Velocity vectors of different flow surfaces at 0.46QBEP1 operating condition (32mm).



**Fig. 13. Streamlines and pressure of different discharge for stay vane outlet on the circumferential section (streamwise 3.7, 32mm)**



**Fig. 14 Streamlines of different discharge for stay vane outlet (32mm)**

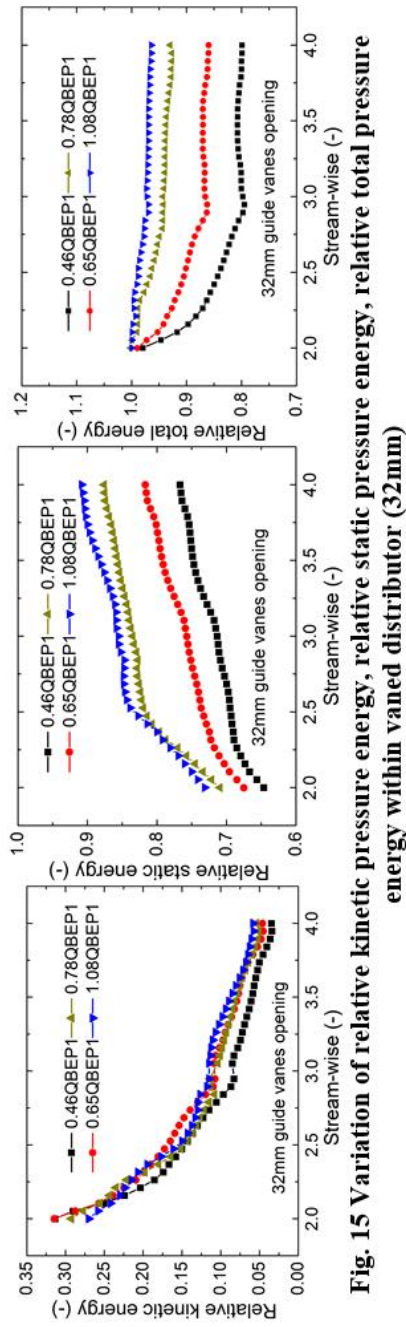


**Fig. 15** Variation of relative kinetic pressure energy, relative static pressure energy, relative total pressure energy within vaned distributor (32mm)

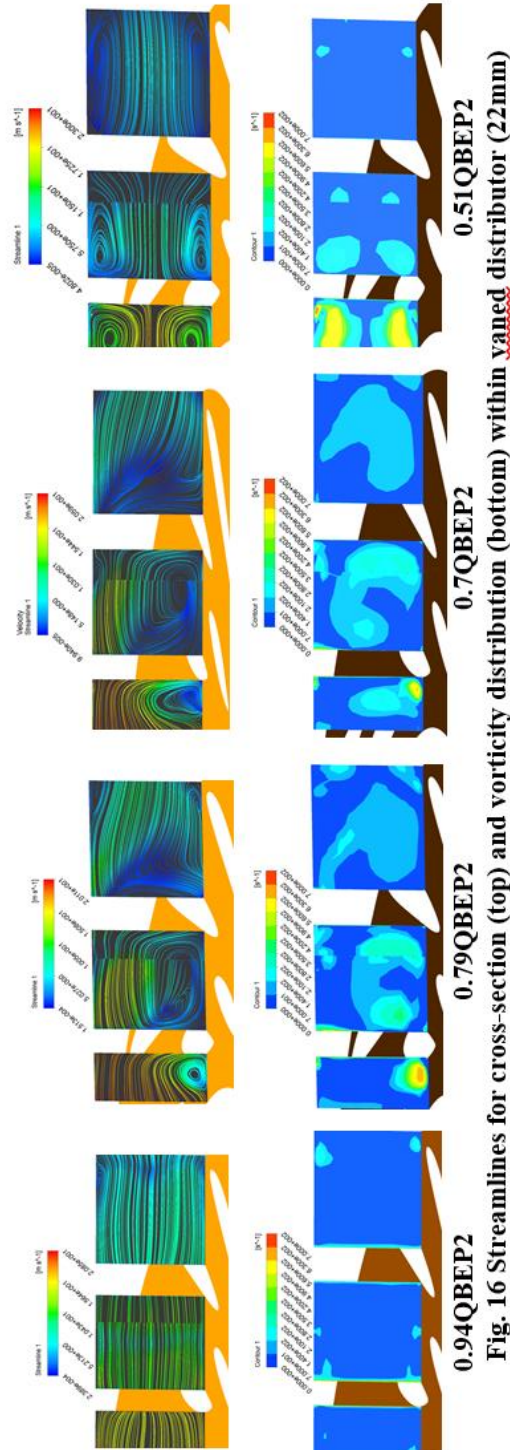


**Fig. 16** Streamlines for cross-section (top) and vorticity distribution (bottom) within vaned distributor (22mm)

outlet was used as a reference. Fig. 15 presents variation of relative kinetic pressure energy, relative static pressure energy, and relative total pressure energy within vaned distributor (32mm). Some conclusions can be obtained from Fig. 15 as follows:

- 1) Along streamwise, relative kinetic pressure energy gradually decreases and converts to relative static pressure energy which gradually increases. However, the relative total pressure energy decreases because of the existing of energy loss.
- 2) When the discharge is reduced, the loss arises, and the ability of converting to relative static pressure drops.
- 3) The total pressure loss within guide vanes is larger than that within stay vanes. Hence, during the small discharge region, losses coming from backflow within guide vanes are larger than ones originated from helical flow within stay vanes.

Under 22mm and 19mm guide vanes openings, the flow pattern within vaned distributor is different from that of 32mm. Figs. 16 and 17 illustrate flow information within vaned distributor under 22mm guide vanes opening. With respect to 0.94QBEP2 of 22mm, the flow field shows smooth, and no obvious vortex could be observed within vaned distributor.

As for the 0.7QBEP2 and 0.79QBEP2 operating condition points, the flow pattern is rather similar. Both backflow and vortex can be founded in the guide vanes inlet, outlet as well as stay vanes inlet, which lead to energy loss and total pressure drop sharply. When the discharge is reduced to 0.51QBEP2, symmetry vortex motion based on the center section near top cover and bottom cover could be observed within vaned distributor. Symmetrical vortex motion blocks seriously upstream fluid, converts the kinetic pressure to static pressure rapidly during this section. In addition, the high intension of vortex motion results to total pressure rapid drop. The range and intension of vortex motion gradually decrease after guide vanes inlet, so the energy loss turns small. In a sum, points 0.79QBEP2 and 0.79QBEP2 are in hump region. Backflow and vortex are more obvious and flow pattern is more unstable than other operating conditions, which lead to the intension of the vortex motion change. Point 0.94QBEP2 is near best efficiency point, no obvious backflow and separation can be noted from Fig. 16. The intension of vortex shows very low. Although there are some obvious vortex motions at 0.51QBEP2, the vortexes are all small and symmetrical. This leads the intension of vortex motion small.

Like 22mm guide vanes opening, the energy loss of 18mm (see Fig. 19) mainly occurs in the guide vanes existing vortex motion and backflow. During the hump region, variation of the kinetic energy and static pressure is the same. As for 0.94QBEP3, the energy loss near the guide vanes outlet shows large. When reduced to 0.87QBEP3, the intension of vortex motion between middle section of guide

vanes and stay vanes outlet is obviously lower than that of 0.94QBEP3 and 0.8QBEP3 operating condition points. The range of vortex motion with stay vanes turns small (see Fig. 18). This phenomenon may contribute the head to arising again during the head-discharge external characteristic curve.

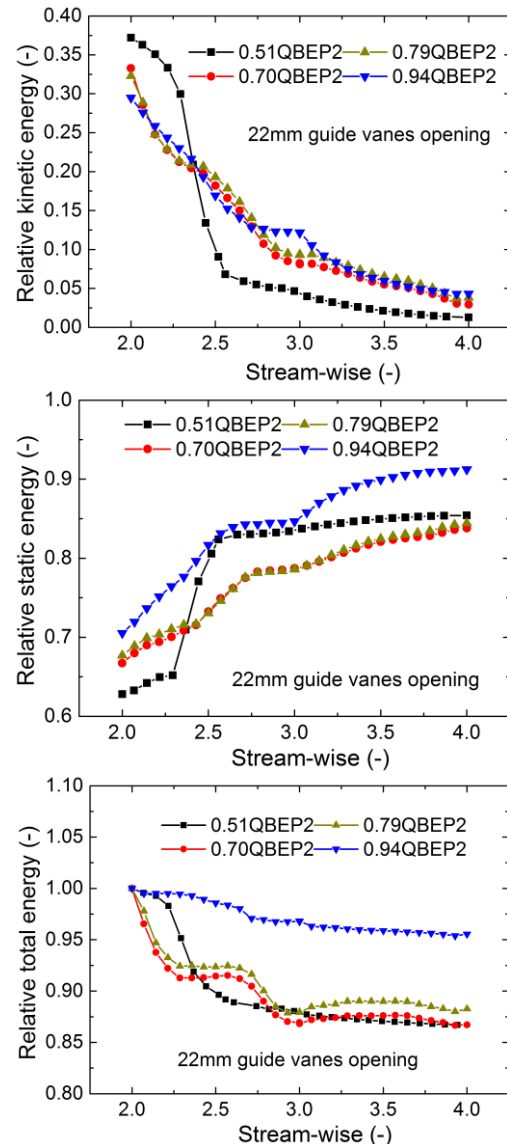


**Fig. 17. Variation of relative kinetic pressure energy, relative static pressure energy, relative total pressure energy within vaned distributor (22mm).**

The inlet section of vaned distributor shown in Fig. 20 is chosen to analyze the energy loss. With decreasing of the discharge, the energy loss increases sharply due to appearing serious backflow and flow separation (see Fig. 21). It is also noted that, with the decreasing of guide vanes opening, the loss during the small discharge region decreases because small opening of guide vanes could better adjust to small discharge. However, the flow pattern turns more confused, which leads to complex variation law for loss with discharge, and appearing the hump characteristic.

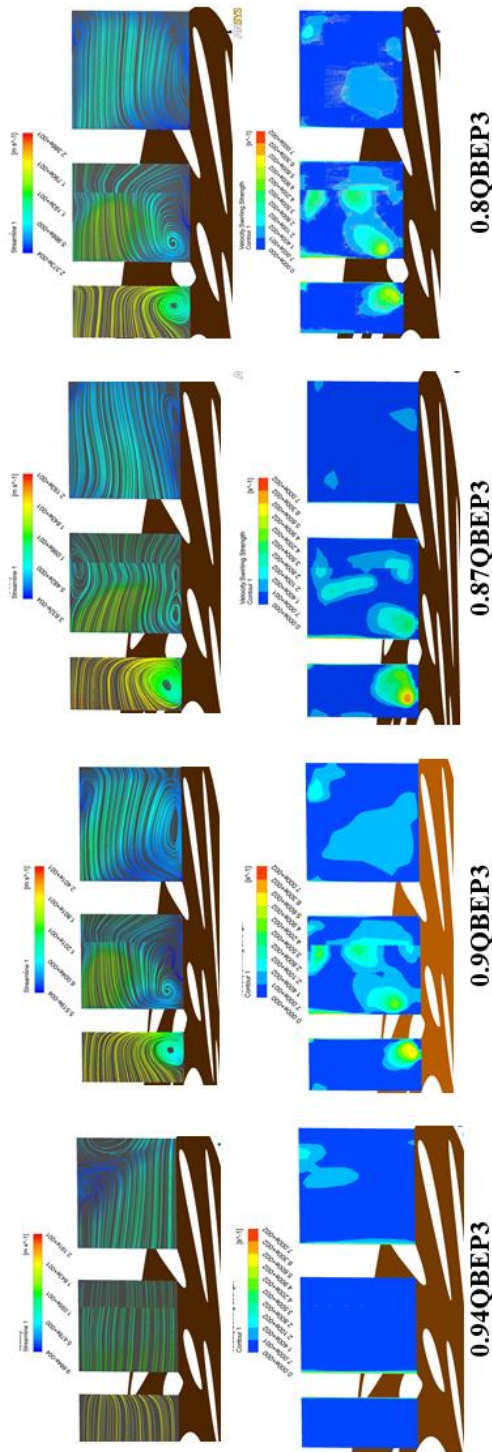


Fig. 18. Streamlines for cross-section (top) and vorticity distribution (bottom) within vaned distributor (18mm)

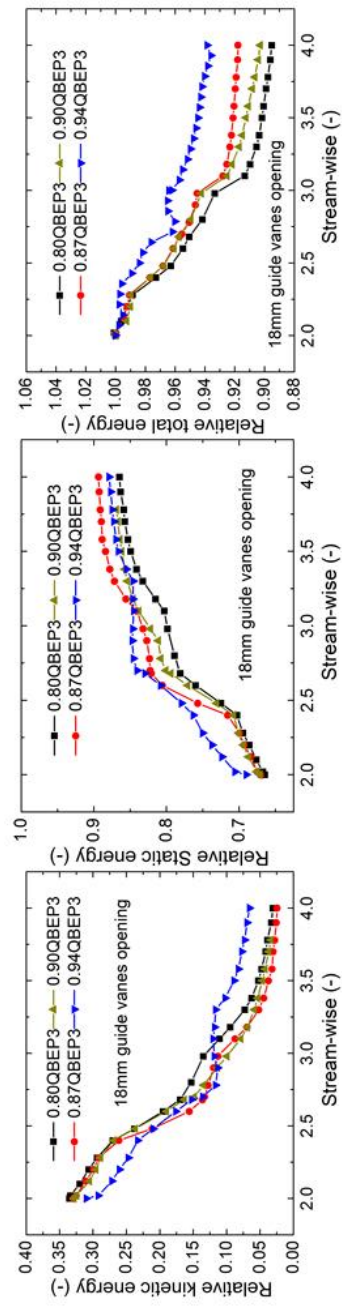
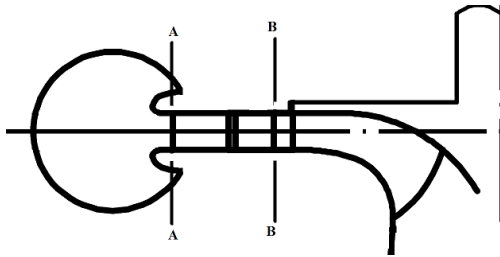
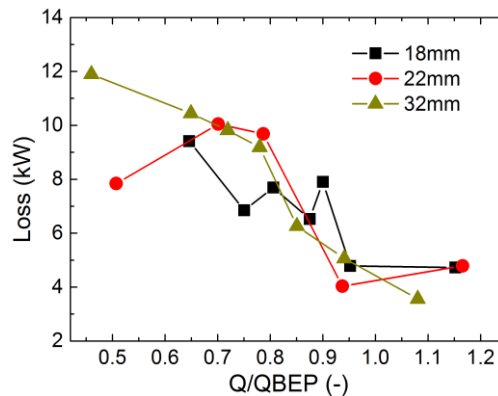


Fig. 19. Variation of relative kinetic pressure energy, relative static pressure energy, relative total pressure energy within vaned distributor (18mm)



**Fig. 20. Schematic diagram for loss analysis within vaned distributor.**



**Fig. 21. Variation of loss within vaned distributor.**

## 5. CONCLUSION

In this research, 3D steady simulations were carried out using different two-equation turbulence models. Compared with the data, SST  $k-\omega$  turbulence model was chosen to performance the external characteristic curves under 32mm, 22mm and 18mm guide vanes openings. The results show a good agreement with the experimental data, especially near the best efficiency points (the error is less than 1.5%). Then the detailed analysis within vaned distributor was carried out under these three guide vanes openings. The variation of flow field, pressure field, energy characteristics and loss distribution within vaned distributor were obtained through the above analysis. As for different guide vanes openings, near the best efficiency point, the flow is smooth and no obvious vortex can be observed. During the small discharge and hump region, the flow becomes complex, secondary and vortex can be found in the vaned distributor. Losses in vaned distributor with discharge under different guide vanes openings show different. The results obtained based on above analysis have a certain value to designer for a pump turbine.

## ACKNOWLEDGEMENTS

This work was supported by the National Key Technology R&G Program (Project No. 2012BAF03B01-X) and Foundation for Innovative Research Groups of the National Natural Science Foundation of China (Grant No. 51121004).

## REFERENCES

- Anciger D., A. Jung and T. Aschenbrenner (2010). Prediction of rotating stall and cavitation inception in pump turbines. *25th IAHR Symposium on Hydraulic Machinery and Systems (Timisoara, Romania, 20-24 September)* (Institute of Physics Publishing)
- Braun O., J. Kueny and F. Avellan (2005). Numerical analysis of flow phenomena related to the unstable energy-discharge characteristic of a pump-turbine in Pump Mode. *2005 ASME Fluid Engineering Division Summer Meeting and Exhibition, Houston, TX, USA.*
- Choi H., M. Zullah, H. Roh, P. Ha, S. Oh and Y. Lee (2013). CFD validation of performance improvement of a 500 kW Francis turbine. *Renew Energy* 54, 111-23.
- Hasmatuchi V., S. Roth, F. Botero, M. Farhat and F. Avellan (2011). Hydrokinetics of a pump-turbine at off-design operating conditions: Numerical simulation. *IOP Conference Series: Earth and Environmental Science* 12 (1) (Hamamatsu, Shizuoka, Japan)
- Int. Energy Agency (IEA) (2012). Technology Roadmap: Hydropower (Paris, France: IEA)
- Liu J., S. Liu., Y. Wu, L. Jiao, L. Wang and Y. Sun (2012). Numerical investigation of the hump characteristic of a pump-turbine based on an improved cavitation model. *Computer and Fluids* 68, 105-111.
- Liu J., Y. Wu and S. Liu (2013). Study of unsteady cavitation flow of a pump-turbine at pump mode. *6th International Conference on Pumps and Fans with Compressors and Wind Turbines, China, Beijing.*
- Li D., H. Wang, G. Xiang, R. Gong, X. Wei and Z. Liu (2015). Unsteady simulation and analysis for hump characteristics of a pump turbine model. *Renewable Energy* 77, 32-42.
- Premkumar T., P. Kumar and D. Chatterjee (2014). Cavitation characteristics of S-blade used in fully reversible pump-turbine. *J. Hydraul. Eng.* 136(5), 051101-01-15.
- Yan J., U. Seidel and J. Koutnik (2012). Numerical simulation of hydrokinetics in a pump-turbine at off-design operating conditions in turbine mode. *26th IAHR Symposium on Hydraulic Machinery and Systems (Beijing, China, 19-23 August)* (Institute of Physics Publishing)
- Yan J., J. Koutnik and U. Seidel (2010). Compressible simulation of rotor-stator interaction in pump-turbines. *25th IAHR Symposium on Hydraulic Machinery and Systems (Timisoara, Romania, 20-24 September)* (Institute of Physics Publishing)
- Yin J., J. Liu and L. Wang (2010). Performance prediction and flow analysis in the vaned

D. Li *et al.* / *JAFM*, Vol. 9, No. 1, pp. 253-266, 2016.

distributor of a pump turbine under low flow rate in pump mode. *Sci. China Tech Sci.* 53(12), 3302-3309.

Zuo Z., S. Liu, Y. Sun and Y. Wu (2015). Pressure

fluctuations in the vaneless space of high-Head pump-turbines—A review. *Renewable and Sustainable Energy Reviews* 41, 965-974.